ACS Catalysis

Research Article

Cite This: ACS Catal. 2018, 8, 968–974

pubs.acs.org/acscatalysis

Artificial Photosynthesis for Formaldehyde Production with 85% of Faradaic Efficiency by Tuning the Reduction Potential

Chang Woo Kim,[†,‡] Myung Jong Kang,[†] Sohyun Ji,[†] and Young Soo Kang*[,†]

[†]Korea Center for Artificial Photosynthesis and Department of Chemistry, Sogang University, #1 Shinsu-dong, Mapo-gu, Seoul 121-742, Republic of Korea

[‡]Department of Graphic Arts Information Engineering, College of Engineering, Pukyong National University, 365, Sinseon-ro, Nam-gu, Busan 48547, Republic of Korea

Supporting Information

ABSTRACT: In the present study, artificial photosynthesis by CO_2 reduction in NaCl is studied for solar fuel production. C1 fuels are evolved from various photoelectrochemical reactions at different reduction potentials depending on the multistep electron-transfer processes to CO_2. The (040) facet engineered $BiVO_4$ (040-BVO)|NaCl|Cu system is illuminated with solar light, and the external bias potential is tuned from 0.7 V to 1.5 (vs RHE) for the CO_2 reduction reaction. Integrating the applied external bias potential into the conduction band minimum of 040-BVO enables the CO_2 molecules to be converted into valuable chemical fuels. This thermodynamic control leads to product selectivity and increased faradaic efficiency. We observed that the selectivity and yield of the products depend on the magnitude of the CO_2 reduction potential. Its products were obtained by tuning the appropriate reduction potential, leading to faradaic efficiencies of 62% for formic acid, 85% for formaldehyde, 8% for MeOH, and 6% for EtOH at different bias in NaCl electrolyte. The correlation between the production of solar chemical fuels and CO_2 reduction potential tuning was studied by applying an external bias potential on 040-BVO|NaCl|Cu. The Cu−C bond distance change during photoelectrochemical CO_2 reduction reaction was investigated with in situ synchrotron X-ray. We suggest that the present results represent the most viable strategy to selectively and efficiently produce solar fuels via artificial photosynthesis.

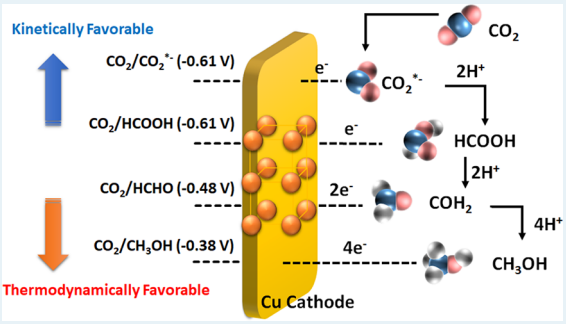

KEYWORDS: *solar energy, solar fuel, water splitting, CO_2 reduction, reduction potential*

INTRODUCTION

Artificial photosynthesis is a conversion process that uses solar light to generate valuable chemical fuels from CO_2 and is currently an innovative research area.[1−3] Together with the hydrogen-evolution reaction (HER),[4] the CO_2-reduction reaction (CO2RR), which emulates natural photosynthesis, produces formic acid (HCOOH), formaldehyde (HCHO), methanol (CH_3OH), and ethanol (CH_3CH_2OH) as liquid fuels and carbon monoxide (CO) and methane (CH_4) as gas-phase products via multielectron shuttling of $2e^-$, $4e^-$, $6e^-$, and $8e^-$ reduction pathways.[5,6] Although these gases are undesirable products because of their potential contributions to climate change, the liquid products produced by the CO2RR are particularly attractive, high-value chemicals because of their high energy density.[7,8] Overall, the CO2RR is an endergonic reaction ($\Delta G^\circ > O$) and involves a series of stepwise processes,[9,10] including the water-splitting reaction for proton and electron production and simultaneous mass-transfer reactions to generate value-added chemical fuels.[11,12] Researchers have attempted to develop CO2RR with high selectivity and yield based on a photochemical (PC) reduction reaction using a molecular/heterogeneous photocatalyst, electrochemical (EC) reduction by an electrolytic cell, and photoelectrochemical (PEC) reduction by a semiconducting photoelectrode.[8,13,14] Together with a hybrid-biocompatible synthetic approach,[15,16] valuable insight from computational investigations and kinetic analyses of the CO2RR have been proposed and reviewed in terms of the thermodynamics.[17−19] The first one-electron-transfer reaction has the highest activation energy barrier, transforming a linear CO_2 molecule to a bent CO_2 radical anion.[20] Further, product selectivity depends on the thermodynamic/kinetic parameters of CO_2 and the intermediates of each step in the reaction.[21] Thus, the development and design of CO2RR devices to achieve the desired selectivity and efficiency for artificial photosynthesis are urgently needed. The proton-assisted multielectron shuttling process of the CO2RR (i.e., a one-pot reduction process) is substantially more energetically favorable when the relatively low redox potentials are considered.[5,6]

Although a multiproton-assisted electron-transfer reaction using abundant electron and hole pairs to drive the relatively low activation energy barrier for the rate-determining step

Received: August 30, 2017
Revised: November 21, 2017
Published: December 19, 2017

DOI: 10.1021/acscatal.7b02953
ACS Catal. 2018, 8, 968−974

under atmospheric conditions was recently proposed, CO2RR remains thermodynamically and kinetically difficult.[22,23] The major challenges associated with the CO2RR include the high selectivity and faradaic efficiency required of its products.[24] Achieving these requirements depends on the catalytic activity of the catalyst, the bias potential applied to the electrode, the dielectric constants of the ionic species, the local pH value in the electrolyte solution, and the concentration of CO_2 in the reactor.[14] Using an EC system, the Bocarsly group proposed a mechanism for the methanol-production reaction using pyridine as a catalyst to lower the activation energy of the first one-electron-transfer reaction.[25] Furthermore, 16 types of CO2RR products were identified in an EC system by the Jaramillo group.[14] In EC/PEC systems, the electrode plays a key role in determining the resulting selectivity and efficiency. Among the metal electrodes used in the experimental processes, copper (Cu) is the only active metallic electrocatalyst that produces formic acid, formaldehydes, and alcohols as major products via the CO2RR.[26,27] However, achieving direct charge transfer to the stable CO_2 molecule requires a high overpotential. Because it is a competitive process, the evolution of hydrogen results in an overall low energy-conversion efficiency.[28] Thus, the high overpotential required and our poor understanding of the parameters of the CO2RR reaction that are critical to control the selectivity of the Cu electrode are significant barriers for the widespread application of this system. The primary hydrocarbon products of CO_2 electroreduction on Cu cathodes have been reported to be methane and ethylene, with negligible methanol formation.[7] Through successive light-harvesting and charge-separation and transport reactions, PEC devices offer a direct semiconductor/liquid interface and suitable energetics for solar fuel production.[1,2,29] Specifically, a coupled photoanode|photocathode system was reported to have 0.14% solar energy-conversion efficiency.[30] Even such tremendous approaches on CO2RR, a selectivity, a yield and a faradaic efficiency on liquid phase-valuable chemical fuels still remain problems to be solved.

Herein, combining a (040)-facet engineered $BiVO_4$ plate photoanode (040-BVO)[31] and a Cu cathode in NaCl electrolyte has been proposed for artificial photosynthesis via the CO2RR. In the PEC CO2RR, a solar-light-driven water-oxidation reaction is performed on 040-BVO, and chemical fuels are produced on the Cu cathode in CO_2-saturated NaCl electrolyte under AM 1.5 G illumination. Tuning the CO_2-reduction potential generates C1 chemical fuels via the multistep electron shuttling process of the CO2RR. The 040-BVO (photoanode)|NaCl (electrolyte)|Cu (cathode) system is illuminated with solar light under an external bias potential that is adjusted to reduce CO_2 by tuning the reduction potential. The present work is focused on two scientific aspects of this system. CO_2 molecules is converted into valuable chemicals by integrating the external bias potential into the conduction band minimum (CBM) of 040-BVO. In this aspect, product selectivity and faradaic efficiency are determined by optimizing the thermodynamic and kinetic parameters of CO2RR. To the best of our knowledge, in this study, the correlation between the selectivity and high yield of the solar chemical fuels via CO_2 reduction by tuning the external bias potential on the 040-BVO has been investigated through in situ synchrotron X-ray analysis on CO2RR. We suggest that the results of this study represent the most viable strategy for developing systems with the desired selectivity and productivity.

RESULTS AND DISCUSSION

A 040-BVO for producing protons (H^+) was hydrothermally synthesized with a $BiVO_4$ seed layer on an FTO substrate using a $TiCl_3$ structure directing agent.[31] Microscopic observations provided information on the growth direction of individual single crystal plates in 040-BVO (Figure 1). High-resolution

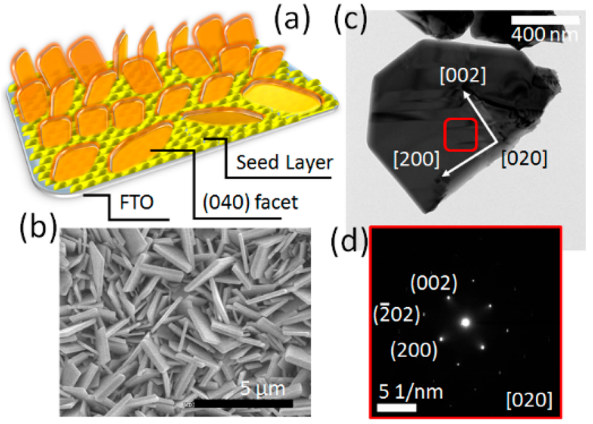

Figure 1. Schematic representation and microscopic observations. (a) Schematic representation, (b) typical top-viewed SEM image, (c) TEM, and (d) SAED pattern of the (040)-crystal facet engineered $BiVO_4$ photoanode. An individual microplate with a lateral (040) facet in the photoanode grew well on the seed layer.

TEM (HRTEM) images and selected area electron diffraction (SAED) patterns viewed along the [020] direction indicate that the $BiVO_4$ microcrystal grew vertically from the $BiVO_4$ seed layer on the FTO. A well-defined individual microcrystal was hydrothermally synthesized as a single crystal plate with 2-exposed (010) crystal facets surrounding 4-exposed (110) and 2-exposed (011) crystal facets in 040-BVO. To better understand the crystal structure of the 040-BVO microcrystal plate, the growth direction from the $BiVO_4$ seed layer was matched along the [121] direction in the monoclinic structure using XRD (Figure S1). The XRD pattern of the 040-BVO diffractions was well indexed to monoclinic scheelite $BiVO_4$ (JCPDS card no. 140688, space group: *I2/a*). The 2θ peak position of the (040) plane in the XRD pattern was located at 30.8°. Because the (040) plane of monoclinic scheelite $BiVO_4$ is positioned with the lateral side of each individual plate, the 2θ value of the lateral side is indistinct in (040)-BVO. Therefore, the peak position of the (040) facet in $BiVO_4$ is related to the exposure of the lateral side facet, as shown in the SEM images (Figure 1b) and XRD pattern (Figure S1a).

PEC CO2RR to solar fuels is a thermodynamically and kinetically unfavorable process. Moreover, its product selectivity depends on the thermodynamic reduction potential tuning of CO_2. The first electron transfer requires a reduction potential of −1.9 eV to reduce CO_2 to its radical anion CO_2^{*-}. Then, a proton-assisted multielectron shuttling process allows the CO2RR to produce C1 fuels with energy barriers from −0.24 eV (vs NHE. Reduction potential for CH_4) to −0.61 eV (vs NHE reduction potential for HCOOH) (Scheme 1a). The protons and electrons that move from the anode compartment to the cathode compartment participate in a one-pot, proton-assisted multielectron shuttling CO2RR reaction at the cathode, during which CO_2 molecules become adsorbed on the surface. Because the electrons transported from the anode are ejected from the Fermi level of the cathode, it is assumed

DOI: 10.1021/acscatal.7b02953
ACS Catal. 2018, 8, 968−974

Scheme 1. Reaction Scheme and PEC CO_2-Reduction Reactor. (a) Schematic Illustrations of 040-BVO-Driven PEC CO_2 Reduction and (b) CO_2-Reduction Reactor for Solar Light-Based Production of Chemical Fuels

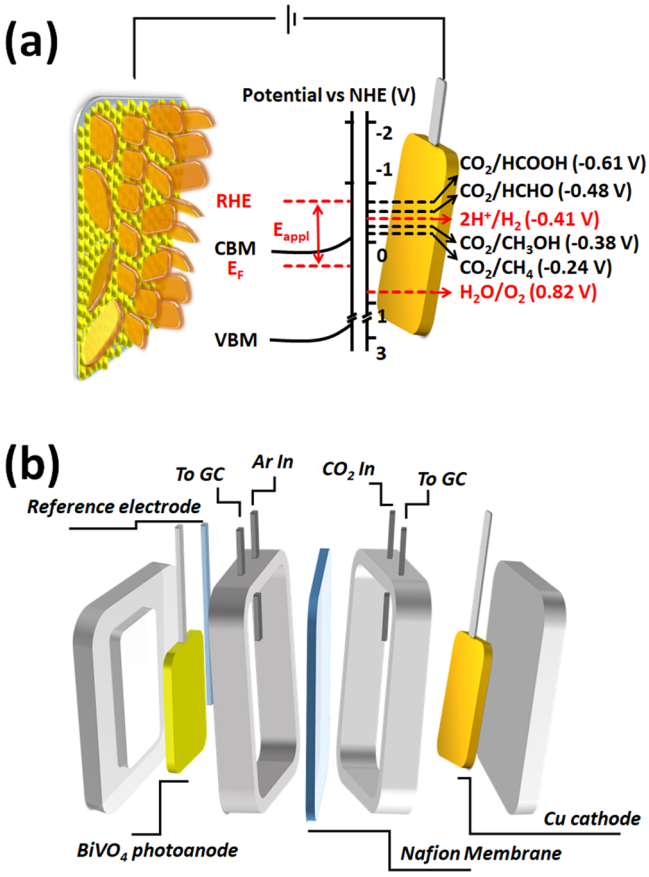

that the reduction potential of the CO2RR can be tuned by applying a bias potential.

As shown in Scheme 1, our strategy for solar fuel production is based on the 040-BVO photoanode driving the multielectron shuttling reduction process for CO_2 by tuning its reduction potential. Based on UV photoelectron spectroscopy (UPS) measurements, the valence band maximum (VBM) of 040-BVO was calculated to be 2.25 eV (vs NHE). From diffuse reflectance measurements (DRS), the band gap (Eg) was determined to be 2.41 eV, and the CBM and Fermi levels were calculated to be 0.16 and 0.6 eV, respectively, by the Mulliken electronegativity theory and UPS analysis suggested by Domen (Figure S2).[32,33] This result show that 040-BVO with more negative VBM can efficiently produce H^+ during water oxidation considering that VBM of typical $BiVO_4$ is located at ~2.4 eV.[34] When 040-BVO is illuminated by solar light, its excited-state electron energy level slightly exceeds the Fermi energy level, which is not sufficient to reduce CO_2. Thus, an external bias potential was applied to increase the Fermi energy and, thus, overcome this gap and tune the potential, thereby adjusting the reduction potential (Scheme 1a). The PEC CO_2 reduction system comprises two compartments that are separated by a Nafion membrane (Scheme 1b). 040-BVO and Cu foil were used as the photoanode (working electrode) and cathode (counter electrode), respectively, and CO_2 gas was continuously bubbled into the NaCl electrolyte. The photocurrent behavior of this system was measured for the CO2RR in Figure 2. Because a typical $BiVO_4$ photoanode exhibits an exponential shaped photocurrent curve, the PEC significance of the 040-BVO|NaCl|Cu system can be determined. The $I-V$ curve has a straight line with a slope, and the high fill factors indicate that the photovoltaic performance in the electrolyte solution allows favorable mass transfer at the semiconductor-electrolyte junction and producing rich H^+.[31] An anodic current with an onset potential of 0.6 V (vs the reversible hydrogen electrode [RHE]) was observed in the CO_2-saturated NaCl electrolyte. Notably, the photocurrent density increased in a stable manner to ~0.1 mA cm^{-2} at 0.75 V, ~0.36 mA cm^{-2} at 0.90 V, ~0.56 mA cm^{-2} at 1.10 V, and ~0.76 mA cm^{-2} at 1.35 V (Figure 2a,b). It should be noted that in NaCl electrolyte, 040-BVO drives the photogenerated charge flow and enhances the charge separation and charge transfer in the water-oxidation kinetics. In our PEC CO2RR system, mass transfer was observed to proceed well with relatively long-term stability.

All CO2RR products were identified and quantified by GC and ^1H NMR spectroscopy using high-performance liquid chromatography (HPLC)-grade standard chemicals (Figures S3 and S4). After the CO2RR in CO_2-saturated NaCl electrolyte in the potential range from 0.7 to 1.6 V (Figure 2c), formic acid, formaldehyde, methanol, and ethanol were detected as liquid products, and hydrogen was observed as a gas product (Figure 2d). Other products, such as CH_4, either were not detected or were present below the detection limits. Formic acid was mainly observed as the CO2RR products at 0.75 V from ^1H NMR spectrum (Figure S5). Compared with the results obtained in N_2-purged conditions, one singlet peak at 8.4 ppm was detected. Based on the chemical shift of a formic acid standard, the main product of the CO2RR at 0.75 V was identified as formic acid. Based on the formic acid calibration curve, approximately 294, 450, and 669 μM formic acid were produced after 5, 7, and 11 h, respectively (Table S1). Strikingly, formic acid was produced at a rate of approximately 61 $\mu M\ h^{-1}$ on the exposed surface of the Cu electrode with a circular area of 1.32 cm^2 (Figure 2d). The products of the CO2RR at 0.90 V was measured by GC (Figure S6). Standard solutions of MeOH, EtOH, and formaldehyde were detected at retention times of 5.8, 7.1, and 7.8 min, respectively (Figure S4). Notably, the GC spectrum of the product of the CO2RR at 0.90 V had a peak at a retention time of 7.8 min that was not present in the spectrum obtained after the N_2-bubbling experiment. On the basis of the formaldehyde calibration curve, approximately 0.56, 0.73, 1.28, and 1.60 μM formaldehyde were produced after 4, 5, 9, and 11 h, respectively (Table S2). Approximately 143.1 $\mu M\ h^{-1}$ of formaldehyde was produced as a main product at 0.90 V in the BVO|NaCl|Cu system (Figure S7). The alcohol products were detected at potentials over 1.15 V. The GC spectrum of the product of the CO2RR at 1.35 V revealed the three peaks detected at retention times of 5.8, 7.1, and 7.8 min were attributed to MeOH, EtOH, and formaldehyde, respectively (Figure S8).

Figure 3 shows the normalized graph of the faradaic efficiencies of the liquid products vs the potential. Following PEC electrolysis, no products were detected below 0.7 V. The faradaic efficiency of formic acid was 65.4% at 0.75 V, yielding a rate of 1.22 $\mu mol\ h^{-1}$. The faradaic efficiency of formic acid decreased as the potential increased to 0.90 V. At potentials between 0.8 and 1.4 V, the faradaic efficiency of formaldehyde demonstrates parabolic behavior. The product selectivity at low potential was presumed to result in the kinetically favorable

DOI: 10.1021/acscatal.7b02953
ACS Catal. 2018, 8, 968−974

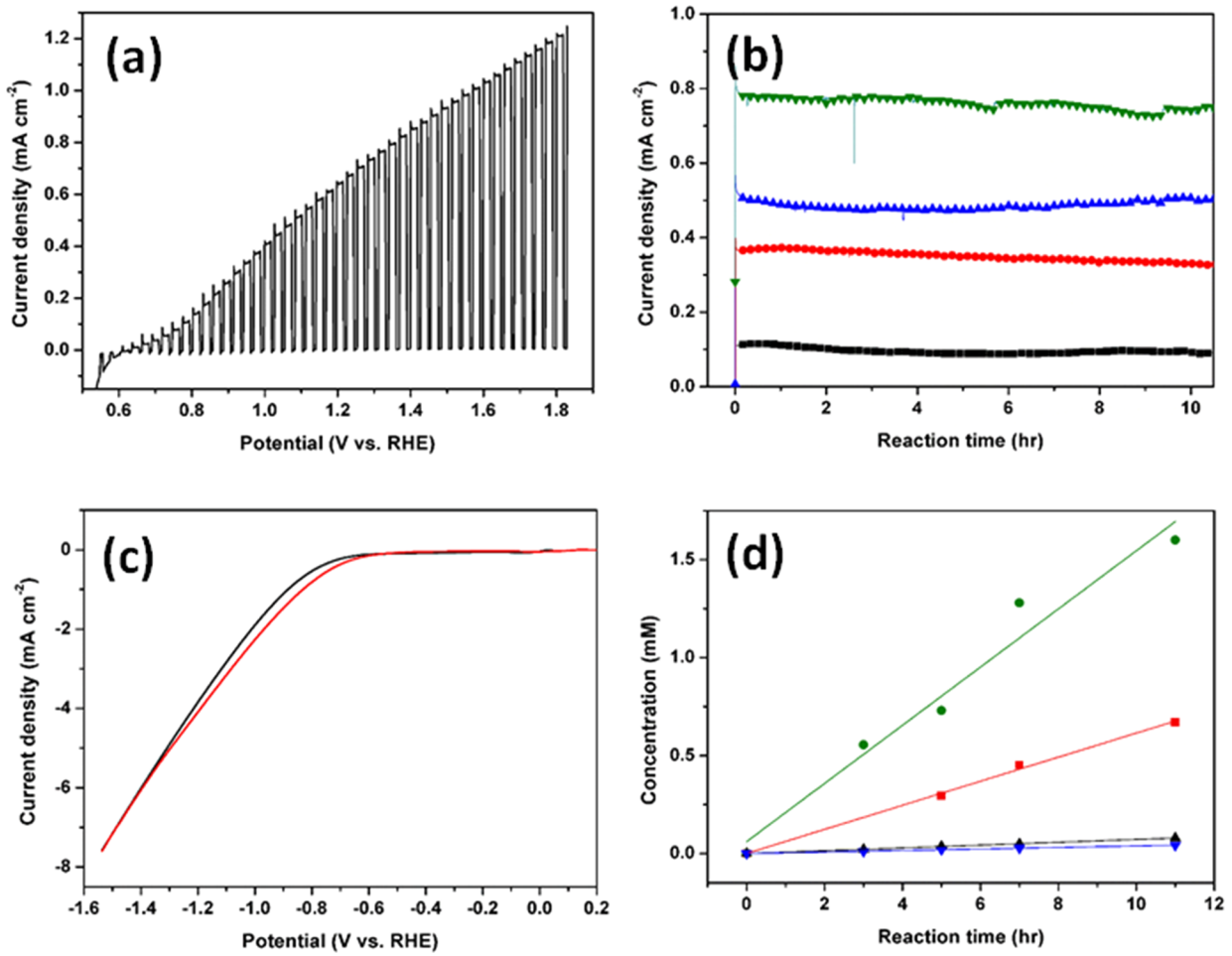

Figure 2. *I*−*V*/*I*−*t*/CV curve and products from PEC CO2RR. (a) Photoresponse of the 040-BVO|NaCl|Cu system, (b) *I*−*t* curves at 0.75 V (vs RHE, black), 0.90 V (red), 1.10 V (blue), and 1.35 V (green) in CO_2-bubbled electrolyte, (c) LSV of Cu cathode (red; CO_2 purged, black; N_2 purged), and (d) time-dependent quantitative analysis of products (green; HCHO at 0.90 V, red; HCOOH at 0.75 V, black; MeOH at 1.35 V, blue, EtOH at 1.35 V).

product because higher concentrations of HCOOH than of HCHO were obtained at lower potentials.

Considering that an industrial formaldehyde is currently produced by catalytic oxidation reaction of MeOH,[35] few reports have investigated the formation of formaldehyde during the CO2RR.[35,36] Notably, the maximum faradaic efficiency for formaldehyde was determined to be 85.1% at 0.90 V, which corresponds to a rate of 2.86 μmol h^{-1}. Therefore, the high yield of formaldehyde produced by the 040-BVO|NaCl|Cu system is quite impressive. Thus, this approach could be an alternative method for the production of formaldehyde, which is not detected when transition metallic electrodes are used. Moreover, even the EC CO2RR with a glassy carbon electrode has been reported to possess a 19% faradaic efficiency.[35] Under an external bias potential of 1.35 V, the production of MeOH and EtOH was observed to exhibit parabolic behavior. Notably, the maximum faradaic efficiency of MeOH was determined to be 6.89% at 1.35 V (with a production rate of 0.245 μmol h^{-1}), and that of EtOH, a minor product, was observed to be 4.4% with a production rate of 0.1 μmol h^{-1} (Table S3 and Figure S9). Based on our observations on the 040-BVO|NaCl|Cu system, we expect that a highly reduced product should be dominant at high potentials, indicating that a thermodynamically stable product is favored. Hydrogen gas was generated rapidly at potentials over 1.3 V (Figure S10). Other gaseous products, such as methane and carbon monoxide, were either not detected or were generated at quantities under the detection limit. The reduction potential tuning investigated here may have scientific significance for developing a consolidated process for the production of formic acid and alcohols. First, CO_2 molecules are reduced to form formic acid with two e^-/h^+ pairs, and then, formaldehyde and MeOH are continuously produced with 4 and 6 e^-/h^+ pairs, respectively. Together with the PEC photocurrent behavior of the potential shown in Figure 2, it can be concluded that the electrons generated as by the reduction potential affect the CO2RR product selectivity. At low potentials, kinetically favorable products would be dominant, whereas at high potentials, thermodynamically stable products would be dominant. Furthermore, no other liquid products were detected under dark conditions. The CO2RR requires electron- and proton-rich conditions. Thus, NaCl should be a useful electrolyte source because of its conductivity.[35] In particular, the presence of chloride ions in the electrolyte solution reduces double-layer capacitance.[37] Any intermediates involved in the generation of the final product should be eliminated by reduction potential tuning during the CO2RR. Therefore, even NaCl electrolyte exhibits acidic pH values, suppressing competitive reactions, such as the HER at the surface of the cathode, unlike other

DOI: 10.1021/acscatal.7b02953
ACS Catal. 2018, 8, 968−974

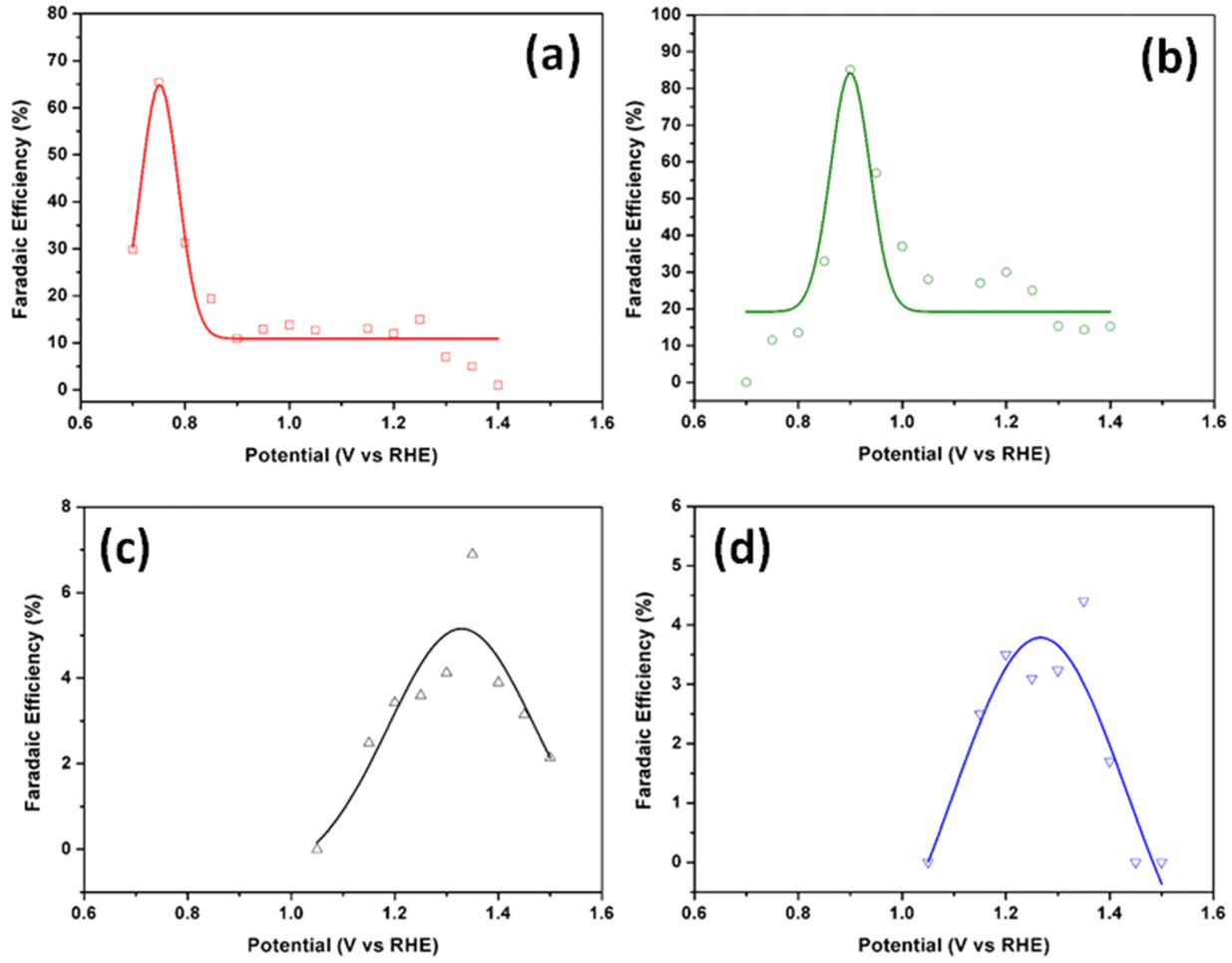

Figure 3. Normalized faradaic efficiency plotted against potential in the 040-BVO|NaCl|Cu system: (a) HCOOH, (b) HCHO, (c) MeOH, and (d) EtOH during CO2RR.

CO2RRs. Figure S11 indicates that CO2RR was carried under constant pH condition in the 040-BVO|NaCl|Cu system.

To prove our hypothesis, in situ X-ray absorption fine structure (XAFS) analysis was performed for the CO2RR using the 040-BVO|NaCl|Cu system (Figure 4). To the best of our knowledge, the X-ray absorption near-edge structure (XANES) and extended XAFS (EXAFS) were first determined to identify the C1 fuel evolution on the Cu cathode during the CO2RR reaction in Figure S12. Based on the EXAFS results (Figure S13), the distance between neighboring Cu atoms under solar light illumination was comparatively studied. In fluorescence mode, the Cu K-edge XANES spectra showed similar results for the CO_2-bubbling and N_2-purging experiments. The XAFS analysis of the Cu cathode with N_2-purging conditions as a blank is shown in Figure S13a and was compared with that of the simulated interatomic Cu−C and Cu−Cu distances in Figure S13b and c. The Cu−Cu and Cu−C bond distances were simulated to be 0.18 and 0.21 nm, respectively, and the XAFS of the Cu cathode under N_2-purging conditions shows a major peak at a distance of 0.21 nm, which matches the simulated XAFS values. Notably, the XAFS spectra for the CO_2-bubbled experiments at 0.65 and 0.75 V (Figure 4), for which the external bias allows formic acid to be evolved from the CO2RR, show two remarkable peaks that correspond to a distance of 0.21 nm and one that is slightly left-shifted. Presumably, mass transfer reduces stable CO_2 molecules to CO_2^{*-} at the Cu cathode because the CO2RR occurs at the surface of this electrode. At 0.90 V, formaldehyde was evolved, and one major peak appears at 0.195 nm, shifted from 0.21 nm. During the alcohol-evolution reaction, two notable peaks appear at 0.18 and 0.21 nm, which correspond to the Cu−C and Cu−Cu bond distances, respectively. These phenomena indicate that mass transfer to CO_2 molecules is stimulated at the surface of the Cu cathode through the Cu−C bond as the external bias increases. The increased number of Cu−C bonds

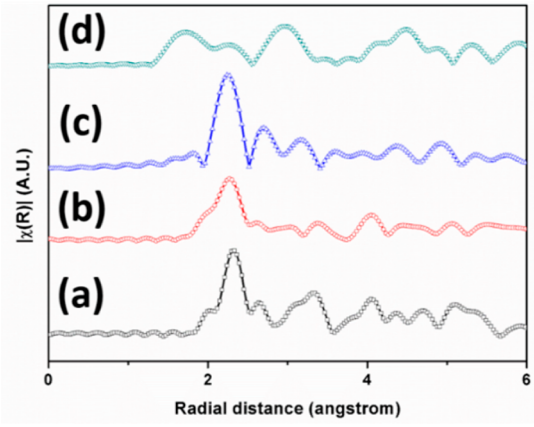

Figure 4. XAFS spectra:. (a) 0.65 V, (b) 0.75 V, (c) 0.90 V, and (d) 1.35 V in the 040-BVO|NaCl|Cu system.

DOI: 10.1021/acscatal.7b02953
ACS Catal. 2018, 8, 968−974

facilitates multielectron shuttling, resulting in the formation of methanol and ethanol.

At the beginning of the CO2RR, the XAFS peak corresponding to the C−Cu bond indicates that carbon approached and adsorbed onto Cu (Scheme 2). Based on the

Scheme 2. Evolved Products from the Cu Surface in the 040-BVO|NaCl|Cu System

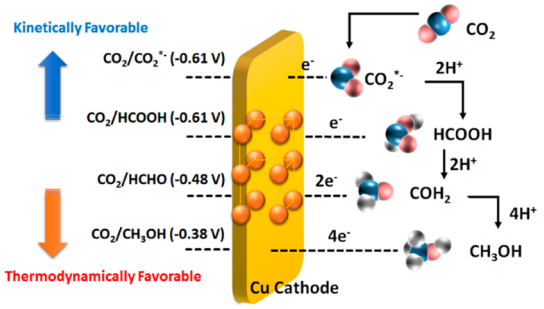

XAFS data for the CO2RR, the atomic bond distance between the Cu atom in the cathode and the C atom in CO_2 decreased as the applied potential was increased. Solar to fuel conversion efficiency (STF) was ∼0.3% of formic acid, ∼ 0.7% of formaldehyde, and ∼0.18% of alcohol at each. Thus, we propose that the 040-BVO|NaCl|Cu system facilitates the formation of sp^2-hybrid carbon atoms for the production of formic acid and formaldehyde at low potentials and that the sp^3-hybrid carbon for the production of alcohol is stable at high potentials.

CONCLUSIONS

In summary, we have demonstrated the use of 040-BVO to drive the CO2RR in NaCl electrolyte by tuning the system's reduction potential. The reduction potential tuning investigated here imply scientific significance for developing a consolidated process for the production of formic acid, formaldehyde, and alcohols. At low potentials, kinetically favorable products would be dominant, whereas at high potentials, thermodynamically stable products would be dominant. This system provides solar fuel product selectivity and yields a high faradaic efficiency for formaldehyde (faradaic efficiencies of 62% for formic acid, 85% for formaldehyde, 8% for MeOH, and 6% for EtOH at different bias). The results reported herein are expected to facilitate increasing the CO2RR efficiency via artificial photosynthesis compared with other approaches and offer valuable insight into the high selectivity and efficiency of the CO2RR.

EXPERIMENTAL SECTION

Electrode Preparation. Synthetic procedure for 040-BVO was slightly modified from that described in our previous report.[31] For the $BiVO_4$ seed layer on the F-doped SnO_2 glass substrate (FTO, TEC-8, 6−9 Ω/sq, 2.0 cm × 2.0 cm), $Bi(NO_3)_3{\cdot}5H_2O$ (5 mmol, 2.4254 g, Sigma-Aldrich, 98%), NH_4VO_3 (5 mmol, 0.5849 g, Sigma-Aldrich), and citric acid (2-hydroxypropane-1,2,3-tricarboxylic acid, 10 mmol, Daejung, Monohydrate 99.5%) were dissolved in 15 mL of 23.3% aqueous HNO_3 (v/v of 60% HNO_3 and distilled water, 0.63/1) and stirred for 30 min. The transparent blue solution was added to acetic acid (3.75 mL) with poly(vinyl alcohol) (PVA, 1.2 g, Aldrich, Mw 89000−98000, 99+% hydrolyzed) and stirred vigorously until the solution became transparent (after approximately 6 h). The solution was dropped and spin-coated onto a clean FTO substrate at 1000 rpm for 20 s and then subjected to heat treatment in air at 723 K for 4 h. In a typical (040)-BVO synthetic procedure, $Bi(NO_3)_3{\cdot}5H_2O$ (4 mmol, 0.1164 g) and NH_4VO_3 (4 mmol, 0.028 g) were dissolved in 60 mL of 2.0 M aqueous HNO_3. Then 0.093 μmol of a titanium(III) chloride solution ($TiCl_3$ in 20−30 wt % HCl, Sigma-Aldrich, 0.12 mL) was added to the solution as a structure-directing agent. After the pH of the reaction solution was adjusted to 0.9 using an ammonia solution (NH_4OH, JIN Chemical, 25−28 wt %), the solution was transferred to a Teflon-lined autoclave (75 mL). The prefabricated $BiVO_4$ seed layer on the FTO substrate was immersed in the reaction solution and allowed to react at 180 °C for 12 h. The hydrothermally reacted substrate was then heat treated at 773 K for 4 h.

PEC Reactor Assembly for the CO_2RR and PEC CO_2 Reduction. A PEC reactor made from transparent glass was assembled with two compartments separated by a Nafion-117 membrane. The anodic compartment was configured with 040-BVO and Ag/AgCl electrodes as the photoanode and reference electrode, respectively. Cu foil was immersed in CO_2-purged, 0.5 M NaCl electrolyte in the counter compartment, which was Tygon-tubed to a gas chromatograph with a column and detector to monitor the gas products. Prior to the CO_2 reduction, the power density of the incident light was adjusted to 100 mW cm^{-2} using a National Renewable Energy Laboratory (NREL)-certified reference cell (Photo Emission Tech., Inc.). The illumination was backside illumination on the FTO surface of the 040-BVO photoanode. The illuminated area had an area of 1.32 cm^2 circle within a 4 cm^2 of 040-BVO photoanode. Cu foil with an equivalent area was used as the counter electrode, and the reference electrode was saturated with 3.0 M KCl. CO_2 was bubbled into the electrolyte at 100 sccm and filled the entire reactor. The PEC CO2RR was performed using a PL-9 potentiostat, and a 300-W Xe arc lamp was used to simulate solar illumination with an AM 1.5 G filter (Asahi HAL-320, 100 mW cm^{-2}) at room temperature and ambient CO_2 pressure.

Quantitative and Qualitative Product Analysis. To analyze the liquid products, a 500 MHz one-dimensional (1D) 1H liquid nuclear magnetic resonance (NMR) spectrometer (Bruker) was used at room temperature (25 °C). The chemical shift was standardized with phenol as the internal reference. A 20 mL aliquot of product-containing electrolyte was added to 10 mL of the standard solution for NMR measurements. The amount of product was calculated from a calibrated standard curve by comparison with the integral area of the product. The qualification and quantification of CO_2 reduction products are measured by gas chromatography (GC) with a purge and trap pretreatment equipment (Figure S14). The 7890B series of GC−FID (Agilent Technologies) equipped with a DB-624 column (60 m × 250 mm × 1.4 mm) and Stratum Purge & Trap (TELEDYNE TEKMAR) was used to analyze liquid products from CO_2 reduction reaction. The injector was operated at constant 200 °C with a He carrier gas (1.5 mL min^{-1}). The oven temperature was held at 40 °C for 1 min and heated to 150 °C by 5 °C min^{-1}, and the detector was operated at 250 °C. Electrolyte samples (5 mL) containing salts were injected into the purge and trap instrument. Injected samples were heated at 40 °C at the same time, and nitrogen gas was purged to the electrolyte by a 40 mL min^{-1} of purging rate. Calibration curves of CO_2 reduction products were obtained by

DOI: 10.1021/acscatal.7b02953
ACS Catal. 2018, 8, 968−974

standard solution of diluted methanol (99.5%, DAEJUNG), ethanol (99.9%, EMD Millipore), and formaldehyde (37% stabilized with methanol, Sigma-Aldrich) solution. The gas product analyses were performed in an airtight continuous-flow cell connected to an online gas chromatography (GC) system (Agilent 7890A) equipped with a pulsed discharged detector (PDD). After the air was removed by He gas (99.9999%) at a flow rate of 6 mL min^{-1} for 3 h in the dark, the working electrode was illuminated under a continuous flow of He at the same flow rate.

■ ASSOCIATED CONTENT

Supporting Information

The Supporting Information is available free of charge on the ACS Publications website at DOI: 10.1021/acscatal.7b02953.

Analysis for ^{1}H NMR, GC, and in situ synchrotron X-ray; additional figures and tables (PDF)

■ AUTHOR INFORMATION

Corresponding Author

*E-mail:yskang@sogang.ac.kr.

ORCID

Chang Woo Kim: 0000-0001-5821-0041

Young Soo Kang: 0000-0001-5746-8171

Author Contributions

Y.S.K. supervised the research project and made a conclusion. Y.S.K. and C.W.K. prepared the manuscript. C.W.K. designed the concept and carried out the PEC measurements. M.J.K. carried out the X-ray absorption measurements and EXAFS analysis during the PEC reaction and GC and NMR measurements. S.J. prepared all of the $BiVO_4$ photoanodes. All of the authors participated in discussions and commented on their interpretations.

Notes

The authors declare no competing financial interest.

■ ACKNOWLEDGMENTS

This work was supported financially by the Korea Center for Artificial Photosynthesis (KCAP) located at Sogang University (No. 2009-0093885), which is funded by the Ministry of Science, ICT, and Future Planning (MSIP) through the National Research Foundation of Korea and the Brain Korea 21 Plus Project 2016. Prof. Dr. Y. S. Kang thanks Dr. M. Kim for performing the experiments at the Pohang Light Source (PLS) supported by MSIP and POSTECH and appreciates the guidance that Prof. Thomas F. Jaramillo and Dr. Christopher Hahn gave us for NMR measurement of products.

■ REFERENCES

(1) Sivula, K.; van de Krol, R. *Nature Rev. Mater.* **2016**, *1*, 15010.
(2) Tachibana, Y.; Vayssieres, L.; Durrant, J. R. *Nat. Photonics* **2012**, *6*, 511−518.
(3) Kim, D.; Sakimoto, K. K.; Hong, D.; Yang, P. *Angew. Chem., Int. Ed.* **2015**, *54*, 3259−3266.
(4) Barber, J. *Chem. Soc. Rev.* **2009**, *38*, 185−196.
(5) Lewis, N. S.; Nocera, D. G. *Proc. Natl. Acad. Sci. U. S. A.* **2006**, *103*, 15729−15735.
(6) Zhu, D. D.; Liu, J. L.; Qiao, S. Z. *Adv. Mater.* **2016**, *28*, 3423−3452.
(7) Nie, X.; Esopi, M. R.; Janik, M. J.; Asthagiri, A. *Angew. Chem., Int. Ed.* **2013**, *52*, 2459−2462.
(8) Kumar, B.; Llorente, M.; Froehlich, J.; Dang, T.; Sathrum, A.; Kubiak, C. P. *Annu. Rev. Phys. Chem.* **2012**, *63*, 541−569.
(9) Luo, W.; Nie, X.; Janik, M. J.; Asthagiri, A. *ACS Catal.* **2016**, *6*, 219−229.
(10) Chen, Z.; Zhang, X.; Lu, G. *Chem. Sci.* **2015**, *6*, 6829−6835.
(11) Marshall, J. *Nature* **2014**, *510*, 22−24.
(12) Wang, W.; Chen, J.; Li, C.; Tian, W. *Nat. Commun.* **2014**, *5*, 4647.
(13) Li, Z.; Luo, W.; Zhang, M.; Feng, J.; Zou, Z. *Energy Environ. Sci.* **2013**, *6*, 347−370.
(14) Kuhl, K. P.; Cave, E. R.; Abram, D. N.; Jaramillo, T. F. *Energy Environ. Sci.* **2012**, *5*, 7050−7059.
(15) Sakimoto, K. K.; Wong, A. B.; Yang, P. *Science* **2016**, *351*, 74−77.
(16) Liu, C.; Colón, B. C.; Ziesack, M.; Silver, P. A.; Nocera, D. G. *Science* **2016**, *352*, 1210−1213.
(17) Zhou, H.; Yan, R.; Zhang, D.; Fan, T. *Chem. - Eur. J.* **2016**, *22*, 9870−9885.
(18) Calle-Vallejo, F.; Koper, M. T. M. *Angew. Chem., Int. Ed.* **2013**, *52*, 7282−7285.
(19) Li, X.; Wen, J.; Low, J.; Fang, Y.; Yu, J. *Sci. China Mater.* **2014**, *57*, 70−100.
(20) Ramesha, G. K.; Brennecke, J. F.; Kamat, P. V. *ACS Catal.* **2014**, *4*, 3249−3254.
(21) Figueiredo, M. C.; Ledezma-Yanez, I.; Koper, M. T. M. *ACS Catal.* **2016**, *6*, 2382−2392.
(22) Kortlever, R.; Shen, J.; Schouten, K. J. P.; Calle-Vallejo, F.; Koper, M. T. M. *J. Phys. Chem. Lett.* **2015**, *6*, 4073−4082.
(23) Centi, R.; Perathoner, S. *Catal. Today* **2009**, *148*, 191−205.
(24) Albo, J.; Alvarez-Guerra, M.; Castaño, P.; Irabien, A. *Green Chem.* **2015**, *17*, 2304−2324.
(25) Yan, Y.; Zeitler, E. L.; Gu, J.; Hu, Y.; Bocarsly, A. B. *J. Am. Chem. Soc.* **2013**, *135*, 14020−14023.
(26) Li, C. W.; Kanan, M. W. *J. Am. Chem. Soc.* **2012**, *134*, 7231−7234.
(27) Raciti, D.; Livi, K. J.; Wang, C. *Nano Lett.* **2015**, *15*, 6829−6835.
(28) Lum, Y.; Kwon, Y.; Lobaccaro, P.; Chen, L.; Clark, E. L.; Bell, A. T.; Ager, J. W. *ACS Catal.* **2016**, *6*, 202−209.
(29) Ji, L.; McDaniel, M. D.; Wang, S.; Posadas, A. B.; Li, X.; Huang, H.; Lee, J. C.; Demkov, A. A.; Bard, A. J.; Ekerdt, J. G.; Yu, E. T. *Nat. Nanotechnol.* **2015**, *10*, 84−90.
(30) Arai, T.; Sato, S.; Kajino, T.; Morikawa, T. *Energy Environ. Sci.* **2013**, *6*, 1274−1282.
(31) Kim, C. W.; Son, Y. S.; Kang, M. J.; Kim, D. Y.; Kang, Y. S. *Adv. Energy Mater.* **2016**, *6*, 1501754.
(32) Butler, M. A.; Ginley, D. S. *J. Electrochem. Soc.* **1978**, *125*, 228−232.
(33) Chun, W.-J.; Ishikawa, A.; Fujisawa, H.; Takata, T.; Kondo, J. N.; Hara, M.; Kawai, M.; Matsumoto, Y.; Domen, K. *J. Phys. Chem. B* **2003**, *107*, 1798−1803.
(34) Park, Y.; McDonald, K. J.; Choi, K.-S. *Chem. Soc. Rev.* **2013**, *42*, 2321−2337.
(35) Nakata, K.; Ozaki, T.; Terashima, C.; Fujishima, A.; Einaga, Y. *Angew. Chem., Int. Ed.* **2014**, *53*, 871−874.
(36) Moriya, I. *Sci. Rep.* **2017**, *7*, 14446.
(37) Quan, F.; Zhong, D.; Song, H.; Jia, F.; Zhang, L. *J. Mater. Chem. A* **2015**, *3*, 16409−16413.

DOI: 10.1021/acscatal.7b02953
ACS Catal. 2018, 8, 968−974